Forecasting Multicycle Hollow Fiber Ultrafiltration Fouling Using Time Series Analysis

Ghadi Dagher, Aurélien Martin, Jean-Michel Galharret, Laurent Moulin, Jean-Philippe Croué, Benoit Teychene

Forecasting Multicycle Hollow Fiber Ultrafiltration Fouling Using Time Series Analysis.

Authors: G. Dagher[1], A. Martin[2], JM. Galharret[3], L. Moulin[2], JP. Croué[1], B. Teychene[1,*]

1. Institut de Chimie des Milieux et Matériaux de Poitiers (IC2MP - UMR CNRS 7285), Université de Poitiers, CNRS, E-BiCOM, 1 rue Marcel Doré, F-86073 Poitiers, France.

2. Eau de Paris, DRDQE, R&D laboratory, 33 Avenue Jean Jaurès, 94200, Ivry-Sur-Seine, France

3. Laboratoire de Mathématiques Jean Leray, UMR 6629 CNRS – Nantes Université, 44000 Nantes, France

Keywords: Time series analysis, exponential smoothing, ultrafiltration, multicycle filtration, membrane fouling prediction.

Highlights

- Multicycle fouling is predicted using exponential smoothing.
- Two models best predict fouling based on observed mechanism.
- Forecasting natural water fouling was successful with small errors.
- Permeability at full-scale was forecasted for 41 days with an error of 3.2%.
- A web application was developed to help apply the new fouling prediction method.

*Corresponding author. Tel: +33549453846. E-mail: benoit.teychene@univ-poitiers.fr

Abstract

This study proposes the application of time series analysis and exponential smoothing (ETS) to predict multicycle membrane fouling with high accuracy and great interpretability. First, lab-scale filtration tests were performed with foulant surrogates to assess the potential of ETS models in predicting multicycle membrane fouling. Two models, ETS(A,A,A) and ETS(A,A,M), were found to be most suitable for describing the variation of transmembrane pressure. The ETS(A,A,A) model showed a slight edge over the ETS(A,A,M) model when reversible fouling was dominant. In contrast, the ETS(A,A,M) performed better when irreversible fouling was prevalent. Then, the effectiveness of ETS models in multicycle forecasting during the filtration of natural water resources was evaluated. Residual mean squared errors between 0.02 bar and 0.15 bar were obtained for horizons going from 2 up to 10 filtration cycles. Finally, ETS models were applied to predict the variation in permeability of drinking water treatment plant membrane skid. A three-month dataset was utilized to predict the next 41 days of permeability variation, yielding an average error of 3.2%. Along with that, a web application designed to assist membrane users in utilizing ETS was developed and presented at the end. The web application can be accessed through the following link: https://fouling-ets.shinyapps.io/shiny-ets-forecasting/.

1. Introduction

Membrane filtration is a widely used technology for drinking water production and wastewater treatment. Despite its effectiveness, membrane fouling is a significant issue that can impair filtration performances, resulting in increased operating costs, energy requirements, and reduced membrane lifespan [1]. Therefore, understanding and predicting membrane fouling is critical to ensure sustainable membrane filtration, and to facilitate the selection of optimal pretreatment conditions to prevent or mitigate membrane fouling [2–5].

In recent decades, there has been a growing interest in predicting and modeling membrane fouling in solid-liquid separation processes [6,7]. Phenomenological models based on hydraulic resistances, transmembrane pressure (TMP), pollutant rejection and other operating parameters have been developed to understand and predict membrane behaviors in solid-liquid separation processes. Charfi et al. [8] developed a mathematical model that predicts multicycle filtration performance based on hydraulic resistances and mass balance of foulant deposition and removal during each cycle. Teychene et al. [9] constructed a model also based on hydraulic resistances to predict the synergistic fouling resulting from the filtration of mixtures comprising particulate matter and NOM. Similarly, Griffiths et al. [10] utilized a network model based on Hermia's models to simulate fouling behavior that allows for the combination of different blocking mechanisms (standard blocking, intermediate blocking…) and fouling caused by particulate adsorption. The study was further extended by Sanaei and Cummings [11], who incorporated the membrane morphology and investigated its impact on separation efficiency and membrane fouling. The models developed in these works and others found in the literature [12] present the advantage of understanding the fouling mechanisms. However, they rely on multiple assumptions about membrane and foulants morphology and structure. Additionally, they require information that is challenging to acquire at an industrial scale which restricts their practical application [11].

Therefore, there is a need to develop more reliable and practical approaches that can overcome the shortcomings of traditional models and accurately predict the performance of membrane processes. The rapid development of artificial intelligence (AI) offers an excellent opportunity to achieve this goal [6,7,13]. With the development of the concept of Industry 4.0, long-term predictions of process performance and the integration of AI strategies into system operations are the subject of a large number of efforts. In particular, due to the complexity of membrane fouling phenomena, the scientific community is currently moving towards data-driven modelling [14–26]. Two main approaches are generally used: (i) The first approach involves using various water quality parameters and operating conditions as inputs for artificial neural networks (ANN) or other AI techniques, which in turn provide the flux or pressure variation as outputs. For instance, previous studies have employed parameters such as TMP, crossflow velocity, pH, feed concentration, filtration time, and operating temperature to predict variables like flux decline or pollutant rejection in the filtration of wastewater [17], oily wastewater [14–16], and milk [23]. The resulting models demonstrated generally high accuracy, with R^2 values exceeding 0.99. (ii) The second approach consists of predicting the variation of TMP (or the permeate flux) using past events. As an example Shim et al. [19] developed a Long Short Term Memory (LSTM) model to predict the value of the next permeate flux (J at time t) of the filtration curves using the four previous data points (J at times t-1, t-2, t-3, t-4). However, despite the advantages of such models, there is a trade-off in terms of interpretability and understanding of fouling mechanisms.

One approach known as time series analysis may offer a solution and present a compromise between the interpretability of mechanistic models and the accuracy of previously mentioned data driven models. Time series analysis involves the examination of data points collected sequentially over time and is usually performed by identifying patterns, trends, and other features that can be used for prediction and decision-making. Similarly to the second

approach explained above (i.e. the LSTM model), previous data points are used to predict future values and variations. Time series analysis encompasses a multitude of methods that fall under the umbrella of AI-based techniques. These methods are widely utilized in diverse fields, from economics to chemical processes, and has recently been applied to membrane filtration [24–27]. The underlying concept behind its implementation in membrane filtration is that the TMP or flux are measured sequentially over time, making it feasible to predict future values based on past data. An example of this implementation was demonstrated by Ruby Figueroa et al. [24]. They employed ARIMA (Auto Regressive Integrated Moving Average) models to predict a 4-hour permeate flux decline in a 10-hour dead-end filtration test without backwashing. In another study, Teychene et al. [26] used an ARIMA(2,1,0) model to forecast the irreversible fouling rate of two underground water resources for a period of 6 months, based on a 12-month database. The advantages of employing these time series models are their simple interpretability, lack of requirement for feed solution or operating conditions data, and their sensitivity to different fouling behaviors, indicating a potential association with membrane fouling. Nevertheless, the previous studies that used ARIMA or ANN models were limited by the use of data coming only from single-cycle filtration tests and did not consider TMP fluctuations observed in multicycle filtration. As a result, these models have limited use in long-term forecasting.

Therefore, the objective of this study is to expand the application of time series analysis to multicycle filtration and develop an algorithm capable of predicting the performance of multicycle filtration, specifically the TMP evolution. To achieve this, experimental data were acquired by conducting lab-scale multicycle filtration tests on synthetic water mixtures and natural water samples. Then a decomposition of filtration curves into trends and seasonal components was performed to get a better understanding of these curves. Afterwards, a time series analysis method called exponential smoothing (or **ETS** which stands for **E**rror **T**rend

Seasonality) was applied on the experimental results. Ultimately, the ETS approach was applied to industrial filtration data. The choice of the time series approach is based on its ability to strike a balance between prediction accuracy and data interpretability, in addition to its ability to be employed on multicycle filtration data. Moreover, ETS models were chosen over ARIMA models because they are more easily generalized and do not require as many assumptions or mathematical constraints (i.e. the presence of unit root [28,29]). In the following, the filtration setup and operating conditions are first described. Then a theoretical description of the ETS models and the developed algorithm are introduced. Finally, the application of these models on multicycle filtration results obtained on various feed water is presented and discussed.

2. Materials and methods

2.1. Feed water and analytical tests

In this study, synthetic feed waters were prepared by dissolving varying concentrations of bovine serum albumin (BSA) (Sigma Aldrich A7906) (ranging from 0 to 5 mgC/L) and sodium alginate (Sigma Aldrich W201502) (ranging from 0 to 5 mgC/L) mixed or not with bentonite (100 mg/L, d_{50}: 2 µm, Na-Montmorillonite, SWy-2, Clay Minerals Society) in MilliQ water (pH 6.8, 18 MΩ.cm at 25 °C). A total of 17 combinations of these three constituents were investigated, inducing different fouling behaviors (both reversible and irreversible). Table S1 provides a detailed list of the 17 combinations investigated. Additionally, surface water samples from the Boivre and Clain rivers in Poitiers, as well as two ground water resources, named Nouvet and Noé exploited by Eau de Paris and used as potential feed water for the “Saint- Cloud” and “L’Haÿ-les Roses” drinking water treatment plants (DWTP) (ultrafiltration process), were utilized in this study. Table S2 provides quality measurements for these resources.

To assess the quality of the water samples, the total organic carbon (TOC), UV absorbance at 254 nm, and turbidity were measured. The TOC analysis was carried out using a TOC-V analyzer from Shimadzu (Japan), while the UV_{254} was measured using a Cary 50 UV-Vis spectrometer from Varian (The Netherlands). Turbidity was measured using a WTW Turb 550 IR Lab Turbidity Meter from WTW (Germany). Additionally, the fluorescence excitation and emission matrix (FEEM) was determined using a FluoroMax 4 spectroflurometer from Horiba (France), with the excitation and emission wavelengths set to a range of 240-500 nm and 290-600 nm, respectively [30].

2.2. Membranes and filtration protocol

Commercial polyethersulfone (PES) hollow fiber membranes (NX Filtration, Netherlands) with a pore size of 0.02 µm, an internal diameter of 0.8 mm and an external diameter of 1.3 mm were used to prepare homemade mini-modules made of 4 fibers of 12 cm potted with epoxy resin (Araldite 2011) and a total membrane surface area of approximately 12 cm^2. The pure water permeability of virgin membranes was equal to 640 ± 90 L/h/m^2/bar (LMHB) at 20°C. Inside-out filtration tests, lasting a total of 24 hours, were carried out on an automated pilot system (as described in Touffet et al. [5]) at a flux of 100 L/h/m^2 (LMH) in one-hour cycles interspersed by 2 min of hydraulic backwash at 200 LMH using the produced permeate. The TMP was measured at 3-minute intervals, resulting in 20 measurement points per cycle. The experiments were automatically terminated when the TMP reached its threshold value of 1.5 bars (even if the 24-hour limit had not been reached). Filtration tests were carried out at temperatures ranging from 18 to 22°C. To ensure the stability of the filtration system, MilliQ water was filtered, and repeatability was assessed by repeating twice filtration tests of randomly selected conditions. The obtained results are presented in Figure S1. The filtration system was deemed stable as no TMP buildup was observed during the filtration of MilliQ water for 24h (Figure S1(a)). Moreover, similar TMP variations were

observed for the repeated conditions, indicating a high level of repeatability. The comparison of filtration curves revealed residual mean square error (RMSE) values ranging from 0.022 to 0.072 bars (Figures S1 (b)-(c)-(d)).

2.3. Fouling indices

Fouling indices are used to quantify and characterize the different fouling behavior observed at lab scale during synthetic suspensions filtration. In this study, fouling indices based on the work of Nguyen et al. [31] were used. These indices have been used extensively in the past and were proven to be good performance indicators of multicycle filtration tests [32–34].

In brief, the total fouling index (TFI) and the hydraulically irreversible fouling index (HIFI) were calculated according to equation 1.

$$\frac{1}{J_s'} = 1 + (FI)V_s \quad (1)$$

Where FI is the considered fouling index (i.e. TFI or HIFI) in units of m^2/L, V_s the specific filtered volume (L/m^2) defined by the permeate volume divided by the membrane surface area and J_s' is the normalized specific flux defined as described in equation 2.

$$J_s' = \frac{\left(\frac{J}{TMP}\right)_v}{\left(\frac{J}{TMP}\right)_0} \quad (2)$$

Thus, under constant flux conditions equation 3 is obtained

$$\frac{TMP_v}{TMP_0} = 1 + (FI)V_s \quad (3)$$

Where TMP_v represents the transmembrane pressure corresponding to a permeate volume V and TMP_0 corresponds to the initial TMP at the start of the experiment.

When TMP_v and V_s are measured between two hydraulic backwashes, the fouling index FI becomes the TFI and can be determined with linear regression if the variation of TMP_v/TMP_0

vs V_s is linear. If it is not linear then the TFI is calculated using the two-point method where only the first and last point of the filtration cycle are used to calculate the slope [32]. HIFI on the other hand can be calculated across multiple filtration cycles with TMP_v and V_s values that corresponds to the start of every filtration cycle. Similarly, to the TFI, linear regression and the two-point method are applied to calculate the HIFI.

2.4. Industrial filtration data

In addition to the laboratory scale filtration tests, industrial filtration data were obtained from one skid (120 modules) on the "L'Haÿ-les-Roses" DWTP operated by Eau de Paris (maximum production 150000 m^3/day). These data were gathered during the period between September 2020 and January 2021 and pertain to an ultrafiltration process that involved different types of membrane cleaning. Among the various cleaning techniques, the most significant one was the chemical backwash with sodium hydroxide, followed by sulfuric acid, which was performed once every 12 days. During the entire operation, the permeability was monitored at intervals of 5 seconds and then reduced to one hour to decrease the size of the dataset. The corresponding data are illustrated in Figure S2.

3. Mathematical background and forecasting methodology

3.1. Data driven model: Exponential smoothing

Exponential smoothing models are forecasting methods for time series first proposed by Brown [35], Holt [36] and Winters [37]. Each model consists of an equation that describes the variation of y_{t+1} (the variable that is forecasted) as a combination of three components and an error. The three components are: (1) l_t the level of the time series at time t, (2) b_t the trend (slope) of the time series at time t, and (3) s_{t+1-m} the seasonal component at time t+1-m where m represents the frequency of the seasonality (i.e. the number of acquired data in one season).

The error ε_t is considered to be normally distributed (i.e. the mean equals to 0 and the variance σ^2 is constant over the considered period).

The level and the error components are always present in the model whereas the trend and seasonal components may be either present or absent depending on the considered model [38]. In general, ETS models' taxonomy are defined by three letters: The first letter represents the error component which can be additive (A) or multiplicative (M), the second letter represents the trend which can be absent (N for none present), additive (A), additive and damped (A_d) or multiplicative (M) and the third letter represent the seasonal component which can be absent (N), additive (A) or multiplicative (M). For example, an ETS(A,A,M) model has an additive error, an additive trend and a multiplicative seasonal component. It is written as follows (Equations 4-7):

$$y_{t+1} = (l_t + b_t)s_{t+1-m} + \varepsilon_{t+1} \quad (4)$$

$$l_t = l_{t-1} + b_{t-1} + \alpha\varepsilon_t / s_{t-m} \quad (5)$$

$$b_t = b_{t-1} + \beta\varepsilon_t / s_{t-m} \quad (6)$$

$$s_t = s_{t-m} + \gamma\varepsilon_t / (l_{t-1} + b_{t-1}) \quad (7)$$

where $\varepsilon_t = y_t - \hat{y}_t$ and $\hat{y}_t$ being the predicted value at time t.

In equation 4, the trend component (b_t) is added to the level component (l_t) whereas the seasonal component (s_{t+1-m}) is multiplied to the other components. Also, the error is added to the equation. The level at time t (l_t) (equation 5), is the sum of the previous level value (l_{t-1}), the value added due to the slope (b_{t-1}) and an error normalized to the seasonal component ($\alpha\varepsilon_t/s_{t-m}$). The other equations (5 and 6) can be understood in a similar fashion. Finally, α, β and γ are three parameters that varies between 0 and 1. They represent the degree of variation between the modeled value and the real value and are estimated using the training dataset. Values that are close to 1 indicate a larger impact of recent observations on future

data (i.e. the last recorded values have a strong impact on future variations, indicating local adaptation for these three components). Conversely, values close to 0 show that older values govern the prediction (i.e. the level, the trend and the seasonal components are global). In total, there are 24 ETS models that corresponds to all the different combinations of error, trend and seasonality. More details about exponential smoothing and innovative state space model (i.e. ETS models) can be found in literature [38,39].

3.2. Forecasting algorithm

In order to forecast the TMP evolution in real time and over multiple filtration cycles a specific algorithm was developed (Figure S3). After acquiring TMP data for a minimal of three cycles (in order to set the seasonal component), an ETS model is selected (choice criteria of selected model to be explained later in section 4.3) and applied to forecast multiple cycles into the future. When a new filtration cycle ends, the entire methodology is repeated. This algorithm utilizes past TMP data as input and predicts future TMP variations as output. The choice of the number of observations for input and output data can be tailored as required. The ETS models and the forecasting algorithm were generated via the R software and the "fpp2" package [40]. This package employs the maximum likelihood to estimate the smoothing parameters α, β and γ, and the initial states l_0, b_0, s_0, s_{-1}, …, s_{-m+1}. The accuracy of the predictions is assessed through the calculation of R^2 and RMSE.

4. Results and discussion

4.1. Filtration performances

The experimental conditions were specifically designed to simulate different fouling behaviors (reversible and irreversible fouling) with varying intensities. To achieve this, three fouling surrogates were tested alone and in different mixtures under constant filtration conditions. The normalized TMP variation ($P-P_0$), along with the corresponding fouling indices TFI and HIFI, are reported for the investigated conditions in Figures 1 and 2.

The filtration of alginate alone (Figure 1(a)), resulted in high irreversible fouling while reversible fouling was smaller and related to the investigated feed concentration. This finding is consistent with the results reported by Chang et al. 2016 [41] when using the permeate for backwash on PES membranes. Moreover, the maximum TMP of 1.5 bar was reached after 19.3 hours of filtration (corresponding to a specific filtered volume of 1930 L/m^2) for 1 mg/L of alginate while higher concentrations of 2 mg/L and 5 mg/L stopped at 11.8 hours (1180 L/m^2) and 4.9 hours (490 L/m^2), respectively. Both HIFI and TFI increased with alginate concentration (Figure 2(a)). Specifically, when 1 mg/L of alginate was used, the HIFI and TFI values were 0.003 m^2/L and 0.005 m^2/L, respectively. These values rose to 0.016 m^2/L and 0.029 m^2/L for 5 mg/L of alginate, respectively. Regarding rejection, alginate was partially rejected by the membrane as TOC rejection varied between 50% and 75%.

Upon filtration of BSA alone, a combination of reversible and irreversible fouling was observed with an increase in reversible fouling over time, as illustrated in Figure 1(b). At the start of the filtration process, a sudden rise in normalized TMP variation (P-P0) was observed, which can be attributed to pore blocking and/or adsorption of BSA on PES membranes as seen in previous works [42,43]. The fouling intensity was found to increase with BSA concentration, as indicated by the TMP reaching 1.5 bars after 7.5 hours (750 L/m^2) and 24

hours for concentrations of 5 mg/L and 2 mg/L, respectively, while the corresponding TMP value for 1 mg/L was only 0.62 bar after 24 hours of filtration. HIFI and TFI (Figure 2(a)) increased as the concentration of BSA increased, from 0.002 m^2/L and 0.008 m^2/L at 1 mg/L to 0.009 m^2/L and 0.027 m^2/L at 5 mg/L. Finally, the TOC rejection of BSA averaged around 73% whereas the UV_{254} rejection averaged around 50%. The removal of BSA was further confirmed through the FEEM spectra shown in figure S4 (a) and (b).

The mixture of alginate and BSA (figure 1(c)) showed a synergic effect as it led to only irreversible fouling that increased with time. This implies that the backwash efficiency is significantly reduced when the two compounds are combined, due to potential adsorption of the foulants on the membrane surface. Similar results on polysaccharide–protein mixtures on ultrafiltration were reported by Susanto et al. 2008 [44] who justified the synergy between alginate and BSA through intermolecular binding. The feed mixture concentration obviously influences the TMP variation. As observed in the 1 mg/L BSA and 1 mg/L alginate mixture, the maximum TMP was achieved after 14.5 h (1450 L/m^2), compared to 8.5 h (850 L/m^2) when the concentrations of the two components were doubled. This influence is further evident in the two mixtures tested, one containing 2 mg/L BSA and 1 mg/L alginate, and the other containing 1 mg/L BSA and 2 mg/L alginate (figure S5 (a)). Both mixtures exhibited similar TMP variations, reaching 1.5 bars after around 10 hours (1000 L/m^2), which falls between the values observed in figure 1(c)). To facilitate further explanations these two conditions, which exhibit the same variation as the curves in figure 1(c), were excluded from the rest of the study. Moreover, HIFI and TFI increased when doubling the concentrations of alginate and BSA from 0.005 m^2/L for both of them to 0.011 m^2/L and 0.018 m^2/L respectively (figure 2(a)). In terms of rejection, TOC and UV_{254} rejections ranged from 50% to 70%. Additionally, the FEEM spectra indicated the elimination of BSA from the mixture, as shown in Figures S6 (a) and (b).

The addition of 100 mg/L of bentonite to the previous investigated suspensions (Figures 1(d), 1(e) and 1(f)) resulted in mostly reversible fouling with larger TMP variations during filtration. Filtration of bentonite suspension alone did not lead to membrane fouling as seen in Figure S5 (b) and had the lowest TFI and HIFI (Figure 2(a)). Moreover, the mixture of bentonite with alginate showed smaller irreversible fouling compared to alginate alone, whereas the addition of bentonite to BSA strongly reduced total fouling resistance and led to highly reversible fouling. The effect of bentonite may be attributed to the adsorption of alginate and BSA on suspended clay particles. This phenomenon has been reported in previous papers [45–47], and it is believed to reduce the adsorption of alginate and BSA on the membrane surface, thereby reducing irreversible fouling. The addition of bentonite had a clear impact on both HIFI and TFI, as demonstrated in Figure 2(a). The HIFI values were notably reduced, and were significantly smaller than the TFI values. The impact of increasing concentrations of alginate and BSA was mostly reflected in the increase of TFI (figure 2(a)). For instance, when the concentration of alginate increased from 2 mg/L to 5 mg/L, the TFI increased from 0.039 m^2/L to 0.080 m^2/L. Similarly, for the BSA and bentonite mixture, the TFI increased from 0.010 m^2/L to 0.015 m^2/L for BSA concentrations of 2 mg/L and 5 mg/L. Finally, when the concentrations of alginate and BSA were doubled (2 mg/L alginate + 2 mg/L BSA + 100 mg/L bentonite), TFI increased from 0.023 m^2/L to 0.040 m^2/L. Regarding membrane rejection, the permeate turbidity consistently remained below 0.5 NTU, which corresponds to rejection rates of over 99% since 100 mg/L of bentonite lead to an average turbidity of 50 NTU. Also, the presence of bentonite did not appear to have any major effect on the removal of TOC and UV_{254}, as their values were similar to those discussed previously.

Upon closer analysis of TFI and HIFI, the filtration curves can be divided into two categories. In the absence of bentonite (Figure 2(a)), HIFI tends to increase with increasing concentrations and is relatively large compared to TFI, indicating that irreversible fouling is the major contributor to the global TMP variation. However, with the addition of bentonite, HIFI is no longer affected by foulant concentrations and becomes relatively insignificant compared to TFI, indicating that reversible fouling becomes much more dominant. Furthermore, the boxplot in Figure 2(b) demonstrates that TFI tends to increase over successive filtration cycles in the absence of bentonite. This is illustrated by the relatively larger length of the boxplots and a wider dispersion of the orange dot points, which represent individual TFI values for every cycle. Conversely, in the presence of bentonite, TFI values remain more constant, which is evident by the smaller length of the boxplots.

To summarize, the filtration curves obtained from the experiments without bentonite can be classified as the first category. In this category, irreversible fouling plays a significant role in total fouling. Due to this, total fouling increases gradually with every filtration cycle. On the other hand, the second category corresponds to the filtration of samples with bentonite where the total fouling is predominantly reversible and remains constant, while irreversible fouling is minimal.

4.2. Time series analysis of filtration curves

As mentioned earlier, since the filtration curves (TMP evolution data) are time dependent, they can be analyzed as time series. Nonetheless, in order to insure the time dependency of TMP data, it is necessary to verify the presence of a correlation between the TMP at a specific time and certain previous TMP values. To do so, the autocorrelation function (ACF) is calculated. Figure 3 presents an example for the curve obtained from the filtration of 2 mg/L alginate and 100 mg/L bentonite, where the correlations between any TMP and the previous 200 TMP measurements (equivalent to 10 filtration cycles) are calculated. The highest ACF

value of 0.88 was observed between TMP values at time t and t-1 (lag = 1). This correlation decreased until it reached the red dotted lines after 8 filtration cycles, below which the correlation was no longer significantly different from zero. Thus, for this filtration curve, TMP values were dependent on the variation of TMP from the last 8 cycles. Furthermore, it is evident that the ACF decrease is not gradual. Instead, there are cyclic spikes in ACF values at multiples of 20 lags, indicating that there is a stronger correlation between TMP values that are obtained at the same time in the previous filtration cycles. Similar results were found for the other curves and some examples are presented in the figure S7. In general, when data exhibit a trend, autocorrelations for small lags tend to be large and positive as observations that are close in time are also similar in size. Hence, ACF plots of trended time series typically have slowly decreasing positive values as lags increase. When data are seasonal, the autocorrelations are higher for the seasonal lags, which are multiples of the seasonal frequency (20 in this case), than for other lags. If the data exhibit both a trend and a seasonal cycle, a combination of these effects is observed. Therefore, the ACF plots support the idea of treating filtration curves as time series with both trend and seasonal cycles.

These components can be visualized through various decomposition techniques. In figure 4, the trend and seasonal components as well as the remainder component are obtained using a classical additive decomposition method. The trend component (Figure 4(b)) which reflects the general movement of the data is seen to be increasing. Its variation is linked to irreversible fouling. The seasonal component (Figure 4(c)) reflects the repeatable pattern between various seasons. In the case of multicycle filtration, it is related to the increase in TMP between the start of every cycle and its end. Finally, the remainder component (Figure 4(d)) represents the unexplained portion of the curve i.e. the remaining data after removing the trend and seasonal components.

As mentioned in the introduction, time series analysis contributes to improving the interpretability and getting a better understanding of filtration curves. Tools such as ACF plots and time series decomposition play pivotal roles in achieving this goal. For instance, when examining the ACF of a filtration curve, significant correlations at specific lags signal robust dependencies between values at those particular time points. In the examples given in this section, strong correlations predominantly aligned with the frequency of hydraulic backwash, underscoring the pivotal role of backwashes in shaping curve patterns. However, if another influencing factor, such as water quality, exhibits consistent variation at a specific frequency, the ACF plot can reveal its impact distinct from backwash effects. High correlations at lags unrelated to backwash frequency indicate the presence of an additional factor, potentially unknown, influencing the filtration curve's variation. Similarly, through time series decomposition, it’s possible to get a better understanding, by distinguishing between the impacts of seasonal occurrences, the overall trend of the curve, irregularities and anomalies, and the unexplained variability or noise in the data.

4.3. ETS modeling of TMP during multicycle filtration tests

After confirming the feasibility of handling filtration curves as times series data with trends and seasonal components, it becomes possible to apply time series modeling techniques on filtration curves. One of the most common methods is the previously explained exponential smoothing. At this stage, it was crucial to assess which ETS models have the ability to effectively model and forecast filtration curves. To achieve this, the filtration curves were divided into training and testing datasets, with the former comprising the initial 75% of the data points. Viable models were then tested on the training portion of each curve, and subsequently used to forecast the testing data, with the corresponding RMSE being calculated.

The viability of ETS models was decided by restricting the choice to certain models that are relevant to multicycle filtration TMP data. Firstly, models containing a multiplicative trend

were removed as they generally provide poor forecasts [38]. Secondly, models with a damped trend were eliminated since they are typically used when the trend is expected to become a flat line in the long term. However, since it is known that the TMP will most likely continue to increase during filtration, the possibility of a damped trend can be dismissed. Models having no trends are eliminated for the same reason. Finally, models with no seasonality were removed as the presence of seasonal variations in filtration curves was confirmed in the previous section (4.2).

Thus, the remaining four models (ETS(A,A,A), ETS(A,A,M), ETS(M,A,A) and ETS(M,A,M)) were tested and compared. The corresponding RMSEs are given in Figure S8. As shown, several models are capable of producing accurate forecasts for each curve. Some curves, such as those involving mixtures of alginate, BSA, and bentonite, can be forecasted with small errors by all models while other curves had varying RMSE values depending on the selected models, such as the examples of 2 mg/L of BSA or 2 mg/L of alginate and 100 mg/L of bentonite. Figure S9, S10 and S11 display the different forecasts for these curves.

The selection of models can be made easier by narrowing down the options to just two models, which can generally describe most of the possible TMP variations. These two models are the ETS(A,A,M) and ETS(A,A,A) models presented respectively in equations 4 and 8.

$$\text{ETS(A,A,A)}: \qquad y_{t+1} = l_t + b_t + s_{t+1-m} + \varepsilon_{t+1} \qquad (8)$$

Both models, ETS(A,A,A) and ETS(A,A,M), share similar components as they both include an additive error and an additive trend which are commonly found in time series [38]. The additive trend is denoted by the "+" sign between l_t and b_t, while the additive error is represented by the "+" sign between ε_t and the remaining equation. However, the main difference between the two models is the type of seasonal component used, which can be either additive or multiplicative. Mathematically, a multiplicative seasonality suggests a

relationship between the seasonal component s_t and the overall trend of the curve represented by $l_t + b_t$. This relationship indicates that the seasonality of the curve will increase or decrease in amplitude based on the overall trend. Conversely, an additive seasonality indicates that the overall seasonality is independent of the values of $l_t + b_t$.

As previously mentioned, the filtration curves can be divided into two categories: the first category with TFI values that increase with the accumulation of irreversible fouling, and the second category where TFI values remain constant regardless of the irreversible fouling. By referring to the theoretical explanation of ETS equations, it is possible to assign the ETS(A,A,M) model to the filtration curves of the first category since there is a relationship between the curve's trend (i.e., the evolution of irreversible fouling) and the seasonal variation represented by the TFI. Similarly, the ETS(A,A,A) can be assigned to the curves of the second category where total fouling is independent of irreversible fouling. The remaining two models (ETS(M,A,A) and ETS(M,A,M)) can still be used, nonetheless, they were disregarded as they do not present any additional information and have larger confidence intervals for their forecasts compared to the ETS(A,A,A) and ETS(A,A,M) models. For that, when dealing with new, unseen data, it is advisable to narrow down the model options to ETS(A,A,A) and ETS(A,A,M) models only. The versatility of ETS models in adapting to fouling behavior represents an additional aspect of interpretability achieved through time series analysis. In cases where fouling behavior is not as evident as the examples illustrated in this study, both ETS models can be tested. The model with superior performance provides insight into the dominant fouling behavior.

Lastly, it's important to note that apart from ETS models, ARIMA models were also examined. In general, good forecasts were achieved with ARIMA, which isn't surprising since many ETS and ARIMA models share an equivalence relationship [38]. Nonetheless, ARIMA models encounter certain mathematical constraints, particularly concerning stationarity [28,

29]. These limitations make it challenging to apply a single ARIMA model universally across all filtration curves. For these reasons, the decision was made to focus solely on ETS models in this study and exclude ARIMA models.

4.4. Multicycle forecasting of natural water filtration

Based on these findings, it is now feasible to apply the forecasting algorithm to predict the variation in TMP during the filtration of natural water. Figure 5 demonstrates this application using Nouvet resource filtration as an example. Specifically, after 6 hours of filtration (Figure 5(a)), an ETS(A,A,M) model was developed from the recorded data. The training data is represented in black, and the model fit is depicted in red. Utilizing this model, 6-hour forecasts were generated (depicted in yellow) with 95% prediction intervals. These forecasts were then compared to filtration data recorded between 6 and 12 hours (shown in grey), serving as testing data. This comparison yielded an RMSE of 0.09 bar and an R^2 of 0.83 as displayed in figure 5(b).

The same analysis was replicated, and ETS(A,A,M) models were created for training data corresponding to 12 and 18 hours of filtration (Figure 5(c) and (e)). Similarly, forecasts were produced for the subsequent 6 hours and compared with testing data spanning the same period. Remarkably low forecasting errors persisted even after 6 hours, with RMSE values of 0.07 and 0.08 bar and R^2 values of 0.91 and 0.82 observed at 12 and 18 hours, respectively (Figure 5(d) and (f)).

It's important to highlight that both ETS(A,A,M) and ETS(A,A,A) models were evaluated, but ETS(A,A,M) was chosen due to its superior performance with lower errors. This selection aligns with the earlier discussion, since the filtration curve displayed signs of irreversible fouling and an escalating total fouling.

This implementation can be viewed as a real-time forecasting application during filtration on an industrial scale. ETS models are established using available data to predict future TMP variations. The testing data here simulates unseen future data that would be acquired if no intervention is made. Moreover, unlike the earlier example where models and forecasts were generated at fixed intervals (6, 12, and 18 hours), in real application, these models and corresponding forecasts will be generated at the conclusion of each new filtration cycle. As these models can be generated within seconds, real-time forecasting of TMP data becomes feasible.

In addition to that, the current analysis involved a 6-cycle filtration horizon. However, it is feasible to generate forecasts with shorter or longer horizons. Typically, shorter forecast horizons exhibit lower errors and have narrower prediction intervals. Conversely, as the forecast horizon increases, errors tend to increase while prediction intervals grow rapidly wider. The filtration curve depicted in figure 5 did not exhibit this phenomenon; however, it can be distinctly evident in other scenarios, as illustrated in figure S12.

An assessment was conducted on the impact of increasing horizons on the RMSE for all four natural water resources. To this end, forecasts were generated for horizons spanning from 2 to 10 filtration cycles and their corresponding RMSE were computed. Figure S13 depicts the resulting RMSE for different forecasts using models created from 6, 12, and 18 filtration cycles. Consistent with expectations, the error in the forecasts increased with the horizon, although remaining below 0.15 bar even for 10-cycle forecasts. Nevertheless, it is recommended to employ relatively short forecasting horizons (not exceeding six filtration cycles in our specific filtration conditions) based on the observed escalation in RMSE with increasing horizons.

4.5. Bridging the gap: from laboratory to industrial-scale filtration

Having established the feasibility of multicycle filtration on laboratory-scale filtration curves, the scope must now be broadened to include the application of ETS to industrial data. This section will provide a brief overview of an industrial filtration data application, followed by an introduction to a forecasting tool that simplifies the use of ETS with new data.

4.5.1. Application on industrial filtration data

The application of ETS forecasting was previously demonstrated on TMP seasonal data, which consisted of filtration cycles separated by hydraulic backwashes. However, this methodology can also be applied to permeability data and chemical cleaning cycles. In this regard, the ultrafiltration industrial data presented earlier was used for ETS forecasting. This dataset presents a significant upgrade compared to lab-scale curves, as it includes 120 industrial filtration modules, making it inherently noisier. Additionally, fluctuations in water quality over the four-month period contribute to much more variations in the curve. Specifically, during this period, the TOC varied between 0.2 mgC/L and 0.49 mgC/L, the UV_{254nm} ranged between 0.005 cm^{-1} and 0.017 cm^{-1} and the turbidity varied between 0.11 NTU and 7.58 NTU.

As illustrated in figure 6, the model was trained using five filtration cycles of 12 days measured between 19/09/2020 and 25/11/2020 (the seasonality was confirmed by an ACF plot (data not shown). The ETS(A,A,M) model was selected, although both models gave similar results. Forecasts were generated until 05/01/2021, which was 41 days later, and the results demonstrated excellent forecasting ability with an RMSE of 29.9 LMHB which corresponds to a mean average percentage error (MAPE) equal to 3.2%, as depicted in figure S14. During the seventh cycle, a discrepancy is noticeable between the forecasted and actual permeability values. The forecasts failed to capture the stabilization of permeability observed in the filtration cycle starting on 08/12/2020. These disparities could be attributed to

fluctuations in water quality. As a result, ongoing efforts are focused on integrating water quality parameters into the forecasts to more accurately account for such variations.

Finally, it is important to note that the original data was preprocessed by reducing the number of data points and smoothed by a moving average of order 9 prior to the application of ETS forecasting to reduce the noise in the data.

4.5.2. Online tool for ETS forecasting

The ability to forecast TMP (or permeability) variations for multiple filtration cycles presents several opportunities for industrial applications that could reduce fouling and prolong membrane life. One such application could be the planning of preventive membranes cleaning, which could be performed when forecasts exceed a predetermined TMP threshold. To facilitate this process, a user-friendly web application was developed to help membrane users apply ETS forecasting to their filtration data. This application allows users to upload their data, create ETS models and customized forecasts, and download their results. The web application and tutorial are accessible via the following link: https://fouling-ets.shinyapps.io/shiny-ets-forecasting/.

5. Conclusion

In this study, time series analysis was employed to analyze the variation of TMP during multicycle filtration. It was first demonstrated that filtration curves can be decomposed into trends and seasonal components, which enhances their comprehension. Then, TMP values were forecasted using exponential smoothing by utilizing past variations. The results indicated the prevalence of two distinct models: ETS(A,A,A) was attributed to filtration curves dominated by reversible fouling, whereas ETS(A,A,M) was found to be more suitable to forecast curves with irreversible fouling.

The models were applied on filtration curves obtained from lab-scale filtration of natural water resources, resulting in errors ranging from 0.02 bar to 0.15 bar depending on the forecast horizon. These models were then used to forecast the decrease in permeability of full-scale industrial membrane skid (120 modules), using three months of filtration data to predict 41 days of permeability variation with an RMSE of 29.9 LMHB (MAPE of 3.2%). Finally, a user-friendly web application was developed to assist membrane users in utilizing ETS forecasting. Works are currently being done to implement the methodology and use the resulting forecasts as a preventive technique to effectively adjust feed water pretreatment conditions and optimize cleaning frequency.

Acknowledgement

The authors acknowledge financial support from the European Union (ERDF) and Région Nouvelle Aquitaine. This work pertains to the French government program "Investissement d'Avenir" (EUR INTREE, reference ANR-18-EURE-0010). The authors would also like to thank NX Filtration for providing the membranes and the staff of Eau de Paris in charge of water sampling and operating the ultrafiltration DWTPs.

Author Contribution

G. Dagher: Methodology, Experimentation, Analysis, Writing. **A. Martin:** Industrial dataset access, Review and Editing. **JM. Galharret, L. Moulin and JP. Croué:** Review and Editing. **B. Teychene:** Conceptualization, Resources, Methodology, Supervision, Review and Editing.

552

553

554 # 6. References

555 [1] R. H. Peiris, M. Jaklewicz, H. Budman, R. L. Legge, et C. Moresoli, Assessing the
556 role of feed water constituents in irreversible membrane fouling of pilot-scale ultrafiltration
557 drinking water treatment systems, Water Res., 47, no 10, (2013), doi:
558 10.1016/j.watres.2013.03.015.

559 [2] A. Touffet, J. Baron, B. Welte, M. Joyeux, B. Teychene, et H. Gallard, Impact of
560 pretreatment conditions and chemical ageing on ultrafiltration membrane performances.
561 Diagnostic of a coagulation/adsorption/filtration process, J. Membr. Sci., 489, 284‑ 291,
562 (2015), doi: 10.1016/j.memsci.2015.04.043.

563 [3] A. Touffet, Impact de la qualité de la ressource, des prétraitements et des lavages
564 chimiques, These de doctorat, Poitiers, 2014. Consulté le: 26 février 2021. [En ligne].
565 Disponible sur: https://www.theses.fr/2014POIT2340

566 [4] C. D. Peters, T. Rantissi, V. Gitis, et N. Hankins, Retention of natural organic matter
567 by ultrafiltration and the mitigation of membrane fouling through pre-treatment, membrane
568 enhancement, and cleaning - A review, J. Water Process Eng., 44, 102374, (2021), doi:
569 10.1016/j.jwpe.2021.102374.

570 [5] W. Gao et al., Membrane fouling control in ultrafiltration technology for drinking
571 water production: A review, Desalination, 272, no 1, Art. no 1, (2011), doi:
572 10.1016/j.desal.2011.01.051.

[6] M. Bagheri, A. Akbari, et S. A. Mirbagheri, Advanced control of membrane fouling in filtration systems using artificial intelligence and machine learning techniques: A critical review, Process Saf. Environ. Prot., 123, 229‑ 252, (2019), doi: 10.1016/j.psep.2019.01.013.

[7] C. Niu, X. Li, R. Dai, et Z. Wang, Artificial intelligence-incorporated membrane fouling prediction for membrane-based processes in the past 20 years: A critical review, Water Res., 216, 118299, (2022), doi: 10.1016/j.watres.2022.118299.

[8] A. Charfi, H. Jang, et J. Kim, Modelling tool to assess membrane regeneration by periodical hydraulic cleaning and fouling control in pressurized membrane process for surface water treatment, Environ. Earth Sci., 78, no 1, Art. no 1, (2019), doi: 10.1007/s12665-018-8011-4.

[9] B. Teychene, G. Collet, et H. Gallard, Modeling of combined particles and natural organic matter fouling of ultrafiltration membrane, J. Membr. Sci., vol. 505, (2016), doi: 10.1016/j.memsci.2016.01.039

[10] I. M. Griffiths, A. Kumar, et S. Stewart, A combined network model for membrane fouling, J. Colloid Interface Sci., 432, 10‑ 18, (2014), doi: 10.1016/j.jcis.2014.06.021.

[11] Sanaei et L. J. Cummings, Flow and fouling in membrane filters: effects of membrane morphology, J. Fluid Mech., 818, 744‑ 771, (2017), doi: 10.1017/jfm.2017.102.

[12] E. Iritani, A Review on Modeling of Pore-Blocking Behaviors of Membranes During Pressurized Membrane Filtration, Dry. Technol., 31, no 2, 146‑ 162, (2013), doi: 10.1080/07373937.2012.683123.

[13] M.-J. Corbatón-Báguena, M.-C. Vincent-Vela, J.-M. Gozálvez-Zafrilla, S. Álvarez-Blanco, J. Lora-García, et D. Catalán-Martínez, Comparison between artificial neural

networks and Hermia's models to assess ultrafiltration performance, SePurif. Technol., 170, 434‑ 444, (2016), doi: 10.1016/j.seppur.2016.07.007.

[14] R. Badrnezhad et B. Mirza, Modeling and optimization of cross-flow ultrafiltration using hybrid neural network-genetic algorithm approach, J. Ind. Eng. Chem., 20, no 2, Art. no 2, (2014), doi: 10.1016/j.jiec.2013.05.012.

[15] R. Soleimani, N. A. Shoushtari, B. Mirza, et A. Salahi, Experimental investigation, modeling and optimization of membrane separation using artificial neural network and multi-objective optimization using genetic algorithm, Chem. Eng. Res. Des., 91, no 5, Art. no 5, (2013), doi: 10.1016/j.cherd.2012.08.004.

[16] B. Rahmanian, Application of experimental design approach and artificial neural network (ANN) for the determination of potential micellar-enhanced ultrafiltration process. Journal of Hazardous materials, (2011), vol. 187, no 1-3, 67-74, https://doi.org/10.1016/j.jhazmat.2010.11.135

[17] S. A. Mirbagheri, M. Bagheri, Z. Bagheri, et A. M. Kamarkhani, Evaluation and prediction of membrane fouling in a submerged membrane bioreactor with simultaneous upward and downward aeration using artificial neural network-genetic algorithm, Process Saf. Environ. Prot., 96, 111‑ 124, (2015), doi: 10.1016/j.psep.2015.03.015.

[18] S. Ghandehari, M. M. Montazer-Rahmati, et M. Asghari, A comparison between semi-theoretical and empirical modeling of cross-flow microfiltration using ANN, Desalination, 277, no 1, Art. no 1, (2011), doi: 10.1016/j.desal.2011.04.057.

[19] J. Shim, S. Park, et K. H. Cho, Deep learning model for simulating influence of natural organic matter in nanofiltration, Water Res., 197, 117070, (2021), doi: 10.1016/j.watres.2021.117070.

[20] F. Chen et al., Pilot-scale investigation of drinking water ultrafiltration membrane fouling rates using advanced data analysis techniques, Water Res., 48, 508‑ 518, (2014), doi: 10.1016/j.watres.2013.10.007.

[21] F. Harrou, T. Cheng, Y. Sun, T. Leiknes, et N. Ghaffour, A Data-Driven Soft Sensor to Forecast Energy Consumption in Wastewater Treatment Plants: A Case Study, IEEE Sens. J., 21, no 4, Art. no 4, (2021), doi: 10.1109/JSEN.2020.3030584.

[22] T. Cheng, F. Harrou, F. Kadri, Y. Sun, et T. Leiknes, Forecasting of Wastewater Treatment Plant Key Features Using Deep Learning-Based Models: A Case Study, IEEE Access, 8, 184475‑ 184485, (2020), doi: 10.1109/ACCESS.2020.3030820.

[23] M. A. Razavi, A. Mortazavi, et M. Mousavi, Dynamic modelling of milk ultrafiltration by artificial neural network, J. Membr. Sci., 220, no 1, Art. no 1, (2003), doi: 10.1016/S0376-7388(03)00211-4.

[24] R. Ruby-Figueroa, J. Saavedra, N. Bahamonde, et A. Cassano, Permeate flux prediction in the ultrafiltration of fruit juices by ARIMA models, J. Membr. Sci., 524, 108‑ 116, (2017), doi: 10.1016/j.memsci.2016.11.034.

[25] J. Wu, Improving Membrane Filtration Performance Through Time Series Analysis. (2021). doi: 10.21203/rs.3.rs-1090774/v1.

[26] B. Teychene, A. Touffet, J. Baron, B. Welte, M. Joyeux, et H. Gallard, Predicting of ultrafiltration performances by advanced data analysis, Water Res., 129, 365‑ 374, févr. 2018, doi: 10.1016/j.watres.2017.11.023.

[27] B. Deng, Y. Deng, M. Liu, Y. Chen, Q. Wu, et H. Guo, Integrated models for prediction and global factors sensitivity analysis of ultrafiltration (UF) membrane fouling:

640 statistics and machine learning approach, SePurif. Technol., 313, 123326, (2023), doi:
641 10.1016/j.seppur.2023.123326.

642 [28] R. J. Hyndman et Y. Khandakar, Automatic Time Series Forecasting: The forecast
643 Package for R, J. Stat. Softw., 27, 1‑ 22, (2008), doi: 10.18637/jss.v027.i03.

644 [29] D. Kwiatkowski, C. B. Phillips, Schmidt, et Y. Shin, Testing the null hypothesis of
645 stationarity against the alternative of a unit root: How sure are we that economic time series
646 have a unit root?, J. Econom., 54, no 1, Art. no 1, (1992), doi: 10.1016/0304-4076(92)90104-
647 Y.

648 [30] G. Coble, Characterization of marine and terrestrial DOM in seawater using
649 excitation-emission matrix spectroscopy », Mar. Chem., 51, no 4, 325‑ 346, (1996), doi:
650 10.1016/0304-4203(95)00062-3.

651 [31] A. H. Nguyen, J. E. Tobiason, et K. J. Howe, Fouling indices for low pressure hollow
652 fiber membrane performance assessment, Water Res., 45, no 8, Art. no 8, (2011), doi:
653 10.1016/j.watres.2011.02.020.

654 [32] M. Zupančič, D. Novak, J. Diaci, et I. Golobič, An evaluation of industrial
655 ultrafiltration systems for surface water using fouling indices as a performance indicator,
656 Desalination, 344, 321‑ 328, (2014), doi: 10.1016/j.desal.2014.04.002.

657 [33] M. Vera et al., Monitoring UF membrane performance treating surface-groundwater
658 blends: Limitations of FEEM-PARAFAC on the assessment of the organic matter role, Chem.
659 Eng. J., 317, 961‑ 971, (2017), doi: 10.1016/j.cej.2017.02.081.

660 [34] C. Ayache et al., Impact of effluent organic matter on low-pressure membrane fouling
661 in tertiary treatment, Water Res., 47, no 8, Art. no 8, (2013), doi:
662 10.1016/j.watres.2013.01.043.

663 [35] R. G. Brown, Statistical forecasting for inventory control. McGraw-Hill, (1959).

664 [36] C. C. Holt, Forecasting seasonals and trends by exponentially weighted moving
665 averages, Int. J. Forecast., 20, no 1, 5‑ 10, (2004), doi: 10.1016/j.ijforecast.2003.09.015.

666 [37] R. Winters, Forecasting Sales by Exponentially Weighted Moving Averages, Manag.
667 Sci., 6, no 3, 324‑ 342, (1960), doi: 10.1287/mnsc.6.3.324.

668 [38] R. J. Hyndman et G. Athanasopoulos, Forecasting: Principles and Practice (2nd ed),
669 2nd edition. OTexts: Melbourne, Australia, 2018. Consulté le: 8 mars 2021. [En ligne].
670 Disponible sur: https://Otexts.com/fpp2/

671 [39] R. Hyndman, A. B. Koehler, J. K. Ord, et R. D. Snyder, Forecasting with Exponential
672 Smoothing: The State Space Approach. Berlin Heidelberg: Springer-Verlag, 2008. doi:
673 10.1007/978-3-540-71918-2.

674 [40] R. Hyndman et RStudio, fpp2: Data for “Forecasting: Principles and Practice” (2nd
675 Edition). 9 septembre 2020. Consulté le: 27 octobre 2021. [En ligne]. Disponible sur:
676 https://CRAN.R-project.org/package=fpp2

677 [41] H. Chang et al., Role of backwash water composition in alleviating ultrafiltration
678 membrane fouling by sodium alginate and the effectiveness of salt backwashing, J. Membr.
679 Sci., 499, 429‑ 441, févr. 2016, doi: 10.1016/j.memsci.2015.10.062.

680 [42] J. Wang, J. Tian, S. Gao, W. Shi, et F. Cui, Dopamine triggered one step
681 polymerization and codeposition of reactive surfactant on PES membrane surface for
682 antifouling modification, SePurif. Technol., 249, 117148, (2020), doi:
683 10.1016/j.seppur.2020.117148.

[43] D. Liu, T. Wang, et C. He, Antifouling polyethersulfone membrane blended with a dual-mode amphiphilic copolymer, J. Mater. Sci., 51, no 16, Art. no 16, (2016), doi: 10.1007/s10853-016-9904-9.

[44] H. Susanto, H. Arafat, E. M. L. Janssen, et M. Ulbricht, Ultrafiltration of polysaccharide–protein mixtures: Elucidation of fouling mechanisms and fouling control by membrane surface modification, SePurif. Technol., 63, no 3, Art. no 3, (2008), doi: 10.1016/j.seppur.2008.06.017.

[45] W. H. Blade et R. Boulton, Adsorption of Protein by Bentonite in a Model Wine Solution, Am. J. Enol. Vitic., 39, no 3, Art. no 3, (1988).

[46] F.-X. Sauvage, B. Bach, M. Moutounet, et A. Vernhet, Proteins in white wines: Thermo-sensitivity and differential adsorbtion by bentonite, Food Chem., 118, no 1, Art. no 1, (2010), doi: 10.1016/j.foodchem.2009.02.080.

[47] X. Sun, C. Li, Z. Wu, X. Xu, L. Ren, et H. Zhao, Adsorption of Protein from Model Wine Solution by Different Bentonites* *Supported by the National Natural Science Foundation of China (No.20466002), the Program of Ministry of Education for New Century Excellent Talents (NCET-04-0989), the Doctor Funds of Xinjiang Bingtuan (04BSZJ04) and the Shihezi University's Key Scientific and Technological Project (ZDGG2004-01)., Chin. J. Chem. Eng., 15, no 5, Art. no 5, (2007), doi: 10.1016/S1004-9541(07)60137-2.

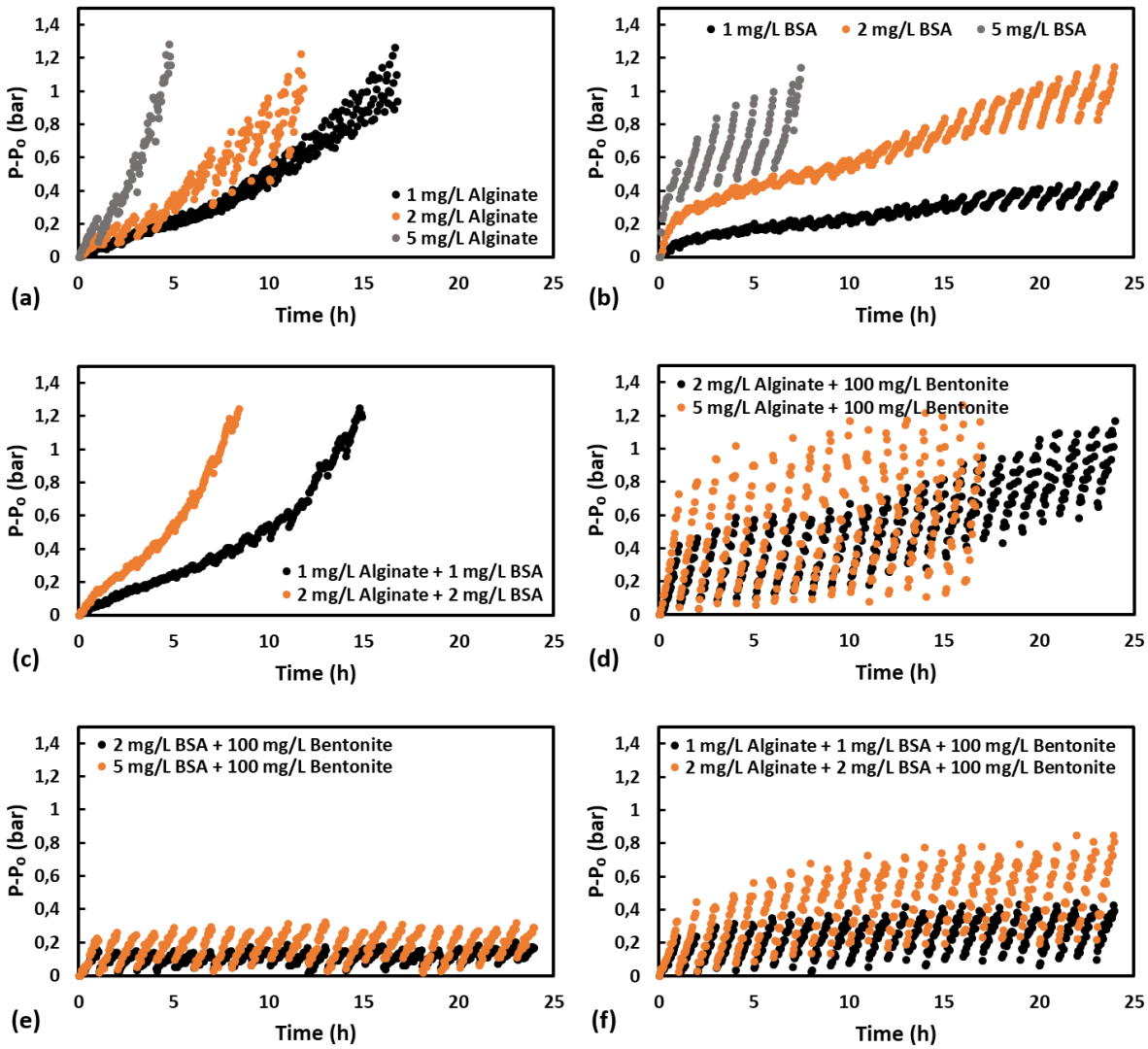

Figure 1: TMP build up during ultrafiltration of synthetic solutions containing (a) alginate, (b) BSA, (c) alginate and BSA, (d) alginate and bentonite, (e) BSA and bentonite and (f) alginate, BSA and bentonite

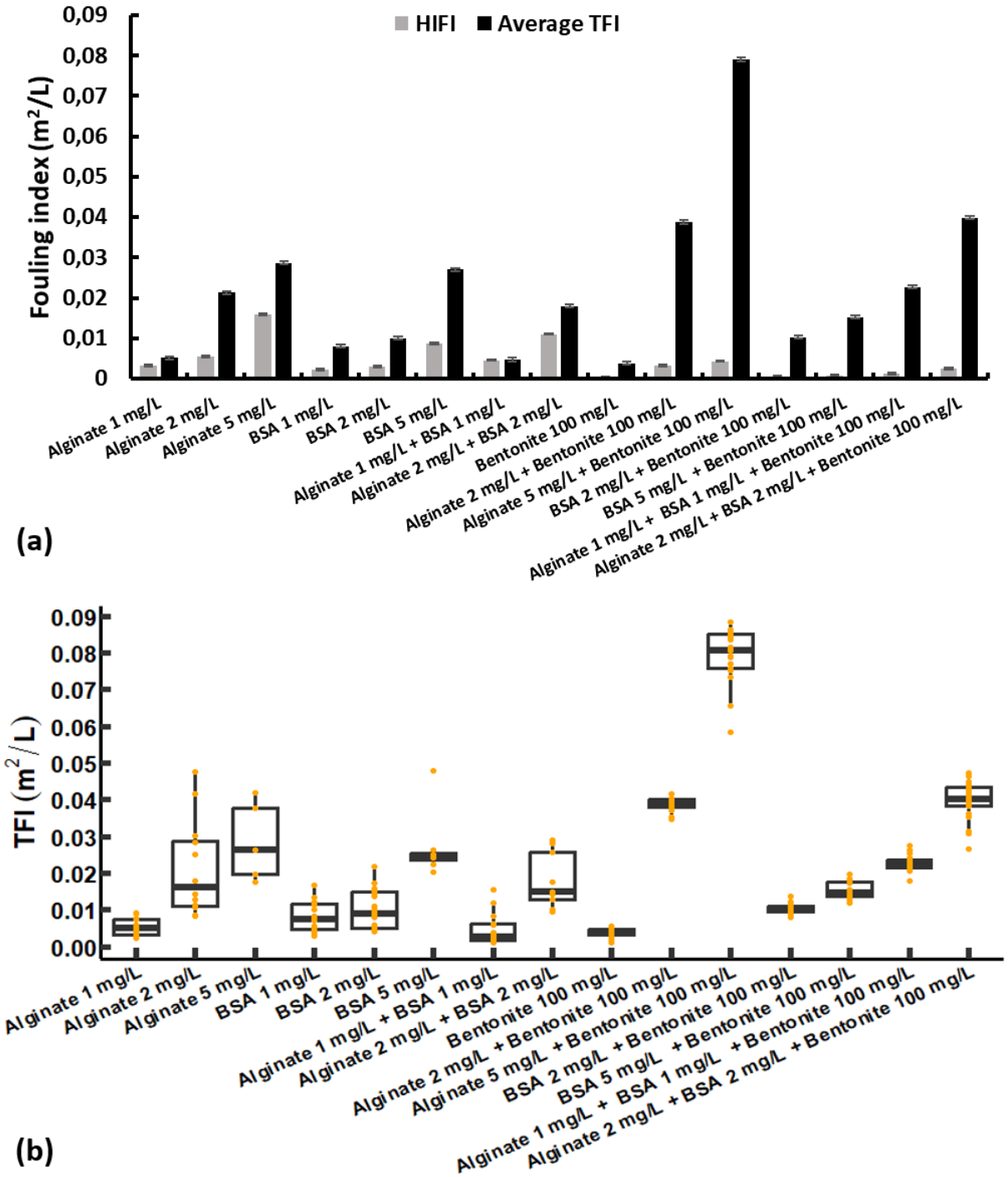

705

706 *Figure 2: (a) Average TFI and HIFI values for tested conditions, (b) Boxplot showing the TFI distribution for*

707 *tested conditions with orange dot points representing TFI values for every filtration cycle.*

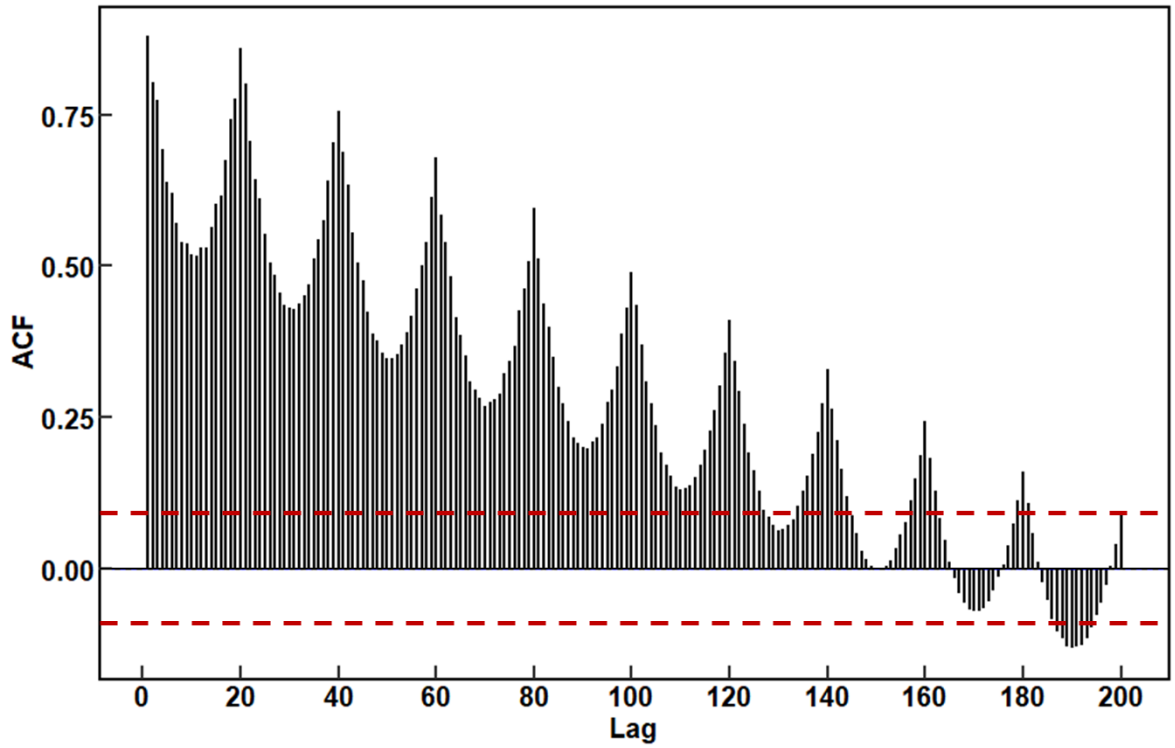

708

709 *Figure 3: ACF plot for the filtration curve obtained from the filtration of 2 mg/L of Alginate and 100 mg/L of*

710 *Bentonite*

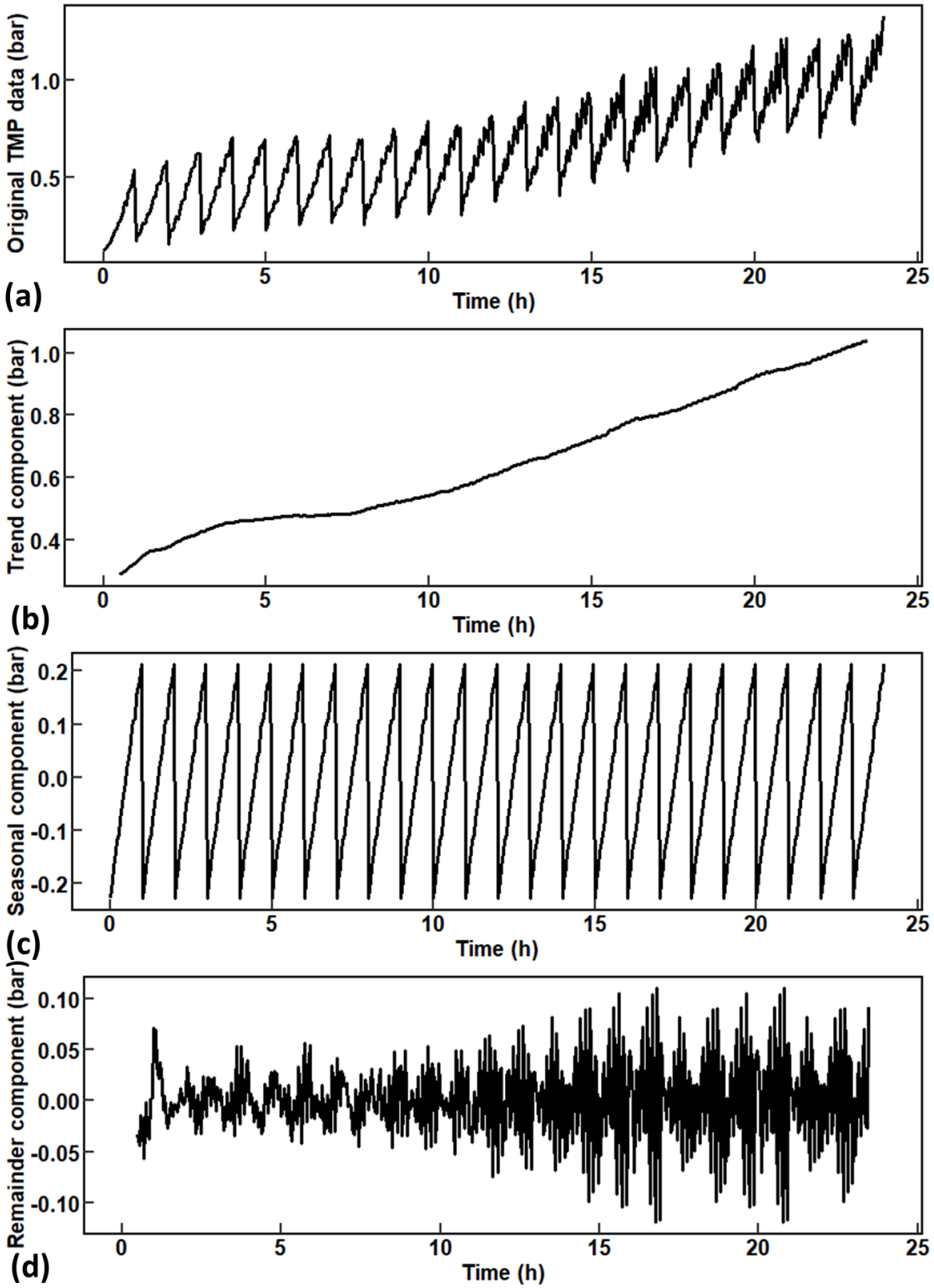

Figure 4: A classical multiplicative decomposition of the filtration curve obtained from the filtration of 2 mg/L of Alginate and 100 mg/L of Bentonite showing (a) the original curve, (b) the trend, (c) the seasonal component and (d) the remainder component.

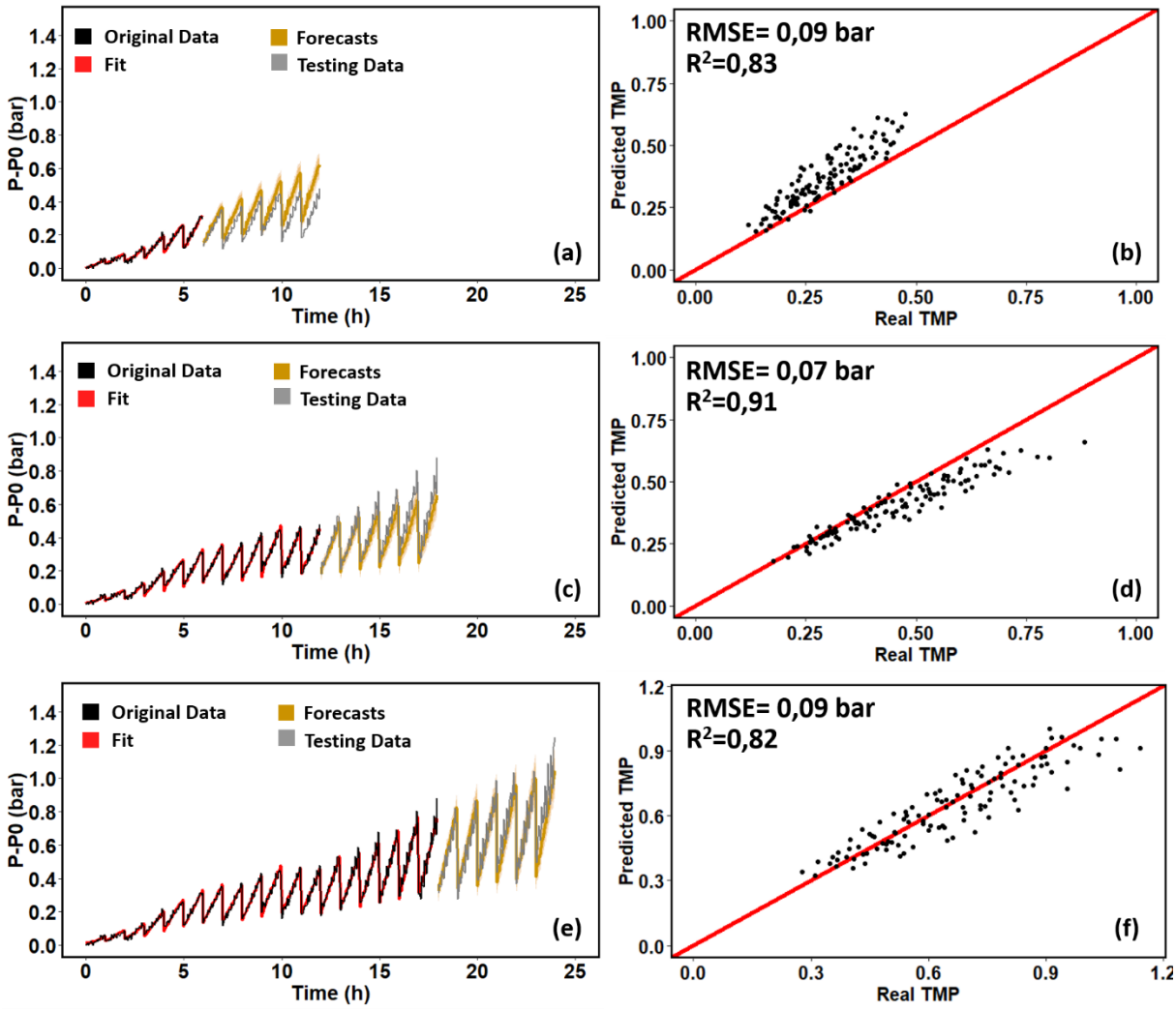

715

716 *Figure 5: (a-c-e) Real-time prediction of the TMP with the actual filtration curve in black (training data), the*

717 *model fit in red, the forecasts with 95% prediction intervals in yellow and testing data in gray, (b-d-f)*

718 *Comparison between the actual pressure and the predicted pressure*

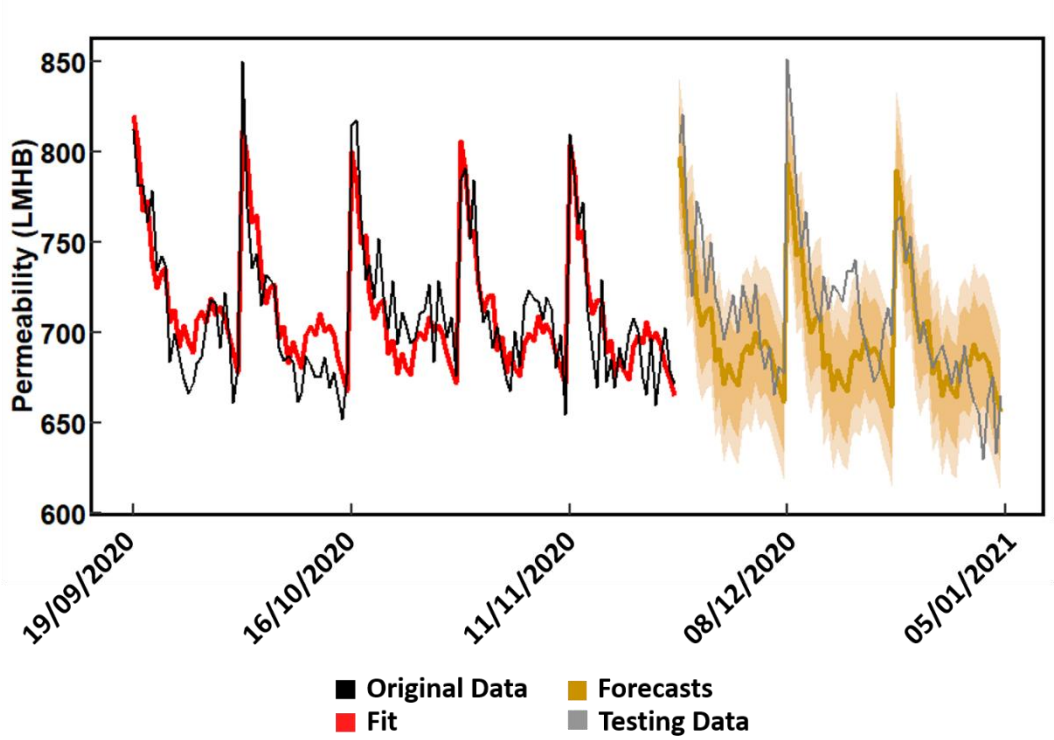

719

720 *Figure 6: Application of ETS forecasting on ultrafiltration industrial data with the smoothed filtration curve in*
721 *black (training data), the model fit in red, the forecasts with both 80% and 95% prediction intervals in yellow*
722 *and the testing data in gray.*